

C. Zucchetti, A. Ballabio, D. Chrastina, S. Cecchi, M. Finazzi, M. Virgilio, G. Isella, and F. Bottegoni, *Probing the in-plane electron spin polarization in Ge/Si_{0.15}Ge_{0.85} multiple quantum wells*. PHYSICAL REVIEW B **101**, 115408 (2020).

DOI: [10.1103/PhysRevB.101.115408](https://doi.org/10.1103/PhysRevB.101.115408)

Probing the in-plane electron spin-polarization in multiple quantum wells

C. Zucchetti,^{1,*} A. Ballabio,¹ D. Chrastina,¹ S. Cecchi,¹
F. Ciccacci,¹ M. Finazzi,¹ M. Virgilio,² G. Isella,¹ and F. Bottegoni¹

¹*LNESS-Dipartimento di Fisica, Politecnico di Milano,
Piazza Leonardo da Vinci 32, 20133 Milano, Italy*

²*Dipartimento di Fisica E. Fermi, Università di Pisa, Largo Pontecorvo 3, 56127 Pisa, Italy*
(Dated: November 14, 2019)

We investigate spin transport in a set of Ge/Si_{0.15}Ge_{0.85} multiple quantum wells (MQWs) as a function of the well thickness. We exploit optical orientation to photogenerate spin-polarized electrons in the discrete energy levels of the well conduction band at the Γ point of the Brillouin zone. After diffusion, we detect the optically oriented spins by means of the inverse spin-Hall effect (ISHE) taking place in a thin Pt layer grown on top of the heterostructure. The employed spin injection/detection scheme is sensitive to in-plane spin-polarized electrons, therefore by detecting the ISHE signal as a function of the photon energy we evaluate the spin-polarization generated by optical transitions driven by the component of the light wavevector in the plane of the wells. Moreover, we gain insight into the electron spin-diffusion length in the MQWs. The sensitivity of the technique to in-plane spin-related properties is a powerful tool to investigate the in-plane component of the spin-polarization in MQWs, commonly hidden.

Group-IV semiconductors offer the opportunity to exploit spin-related features in platforms that are compatible with the mainstream Si-based technology [1–3]. Among them, germanium allows for long spin-diffusion lengths [4–7] and efficient injection [8] and detection of spin-polarized electrons either in Ge itself [9, 10] or in Ge-based heterostructures [11]. The investigation of Ge-based multiple quantum wells (MQWs), thanks to the reduction of the dimensionality, adds peculiar consequences. Indeed, the symmetry reduction produces the appearance of Rashba [12] or Rashba-Edelstein [13] effects. Moreover, quantum confinement and strain effects cause the removal of the degeneracy between heavy-hole (HH) and light-hole (LH) states at the Γ point of the Brillouin zone, which is of particular interest for optical orientation [14, 15]. Indeed, this allows photogenerating a fully-polarized spin population at the Γ point of the conduction band of the well [16]. In the case of Ge/SiGe MQWs this population preserves its spin character on long timescales [17].

It is worth noticing that, at variance from bulk systems, in MQWs the unit vector of the spin polarization \mathbf{u}_P is not parallel to the light wavevector \mathbf{k} [15]. This can be seen either as due to the symmetry reduction in a low-dimensional system or as a consequence of the different probability for optical transitions excited by circularly-polarized electric fields projected normally to the in-plane or the out-of-plane component of the light wavevector \mathbf{k} [18]. Since the most exploited spin-based devices (e.g., magnetic tunnel junctions) mostly deal with in-plane magnetization [19], the knowledge of in-plane spin-polarization P_{\parallel} would be important. However, while it is usually quite simple to directly address the spin-polarization P_{\perp} generated by a light beam im-

pinging out-of-plane the MQWs [16, 17], technical problems in the illumination and the detection process make rather difficult to have access to P_{\parallel} (generated by optical transitions driven by in-plane component of \mathbf{k}). A possible solution of this issue requires the exploitation of planar waveguides based on MQWs [20, 21] which, however, would need to be engineered to be polarization insensitive. Here, we demonstrate that a Pt/MQWs structure can be employed to directly infer from experimental measurement the dependence of the electron spin polarization P_{\parallel} upon the incident photon energy, and thus to determine the effect of the in-plane component of the light wavevector \mathbf{k} on spin-related properties.

In this letter, we investigate the spin transport in Ge/SiGe MQWs for different well thicknesses. Spin-polarized electrons are photogenerated in the discrete conduction levels of Ge wells by exploiting the optical orientation technique [14, 15, 22]. Spins then diffuse towards a thin Pt film grown on top of the MQW structure. Inside Pt, they undergo the inverse spin-Hall effect (ISHE) [23, 24], *i.e.*, a spin-dependent scattering which transforms the optically injected spin current density \mathbf{j}_s into a charge current density \mathbf{j}_c . Following the phenomenological ISHE relation [3] we have:

$$\mathbf{j}_c = \gamma \mathbf{j}_s \times \mathbf{u}_P, \quad (1)$$

with γ being the efficiency of the spin-to-charge conversion. We use Pt as a spin detector due to the large γ value ($\gamma_{\text{Pt}} \approx 0.1$ [25–29]). The ISHE signal is measured under open circuit conditions as a voltage drop ΔV_{ISHE} across two electrodes placed at the edges of the Pt film. Since in this configuration ΔV_{ISHE} is sensitive only to the in-plane component of the spin-polarization normal to the contact direction (P_x) [30–32], we show in the following that the investigation of the inverse spin-Hall effect signal as a function of the impinging photon energy allows to experimentally address the spectral dependence of P_{\parallel} . Notably, our experimental findings are in agree-

* carlo.zucchetti@polimi.it

Sample	t_w (nm)	t_b (nm)	HH1 \rightarrow c Γ 1 (meV)	HH2 \rightarrow c Γ 1 (meV)	LH1 \rightarrow c Γ 1 (meV)	HH3 \rightarrow c Γ 1 (meV)	HH1 \rightarrow c Γ 2 (meV)	HH2 \rightarrow c Γ 2 (meV)
A	10.7	14.8	902 [900]	913 [930]	936 [934]	974 [974]	1016 [1023]	1045 [1053]
B	12.8	17.7	889 [886]	907 [909]	918 [918]	950 [944]	981 [985]	1004 [1007]
C	14.6	20.1	879 [878]	902 [896]	915 [909]	– [924]	956 [960]	977 [978]
D	16.1	22.1	872 [873]	892 [889]	906 [903]	927 [914]	– [947]	954 [962]

Table I. From the left to the right: relevant geometrical parameters of the investigated MQW samples, t_w and t_b being the thickness of the well and the barrier, respectively; values of the optical transitions between discrete energy levels around the direct Ge gap, as extrapolated from the fitting of photoreflectance measurements (see Supplemental Material for further information) and, in square brackets, the results of tight-binding calculations.

ment with the ones computed with a tight-binding approach. This points towards the exploitation of such spin injection/detection scheme as a powerful tool to directly access spin-related properties which are hardly accessible to the common techniques available for spin-polarization measurements.

In Fig. 1 (a) we report the structure of the investigated samples. We employ the low-energy plasma-enhanced chemical vapor deposition (LEPECVD) technique to

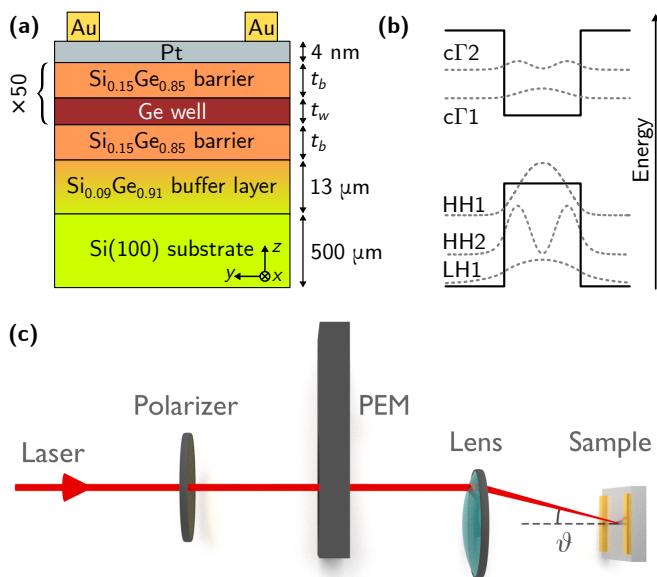


Figure 1. (color online) Samples and experimental geometry. (a) Sketch of the samples. Symbols t_b and t_w represent the thickness of the barrier and the well, respectively, which vary from sample to sample. The spin generation occurs inside the Ge well. Spins are then transferred to the Pt layer. We acquire the electric signal due to spin-to-charge conversion in Pt between two Au contacts. (b) Sketch of the energy levels mostly contributing to optical transitions. (c) Experimental setup.

grow high-quality group-IV heterostructures [33]. On a 500 μm -thick Si(100) substrate, we grow a virtual substrate (thickness: 13 μm), fully relaxed, graded from pure Si to $\text{Si}_{0.09}\text{Ge}_{0.91}$ with a grading rate of 7%/ μm . This serves as a buffer layer for the growth of the first $\text{Si}_{0.15}\text{Ge}_{0.85}$ barrier of the Ge quantum well. Then, we grow 50 periods of Ge wells and $\text{Si}_{0.15}\text{Ge}_{0.85}$ barriers, with well and barrier thicknesses as reported in Tab. I. The structure is then terminated with a 4 nm-thick Pt layer, on which we deposit two Au contacts for the acquisition of the electric signal. The direction between the electrodes [y -axis in Fig. 1 (a)] is parallel to the [110] crystallographic direction of the MQWs. In the following, we name the samples from A to D as a function of the thicknesses of the barrier t_b and of the well t_w , as reported in Tab. I. The table also shows the energy of the direct optical transitions [a sketch of the discrete energy levels is shown in Fig. 1 (b)] that we extrapolate from photoreflectance measurements (see Supplemental Material for details) and the comparison with tight-binding calculations (see below). The agreement between the two is good. Notably, the photoreflectance technique is sensitive also to optical transitions between states of different parity, which are barely visible in transmission [34], and, thus, that do not contribute to the ISHE signal.

To theoretically estimate the energy resolved absorption coefficient and the initial optical polarization spectrum, we used a first-neighbor tight-binding (TB) Hamiltonian description of our Ge/SiGe MQW samples [35, 36]. The semiempirical parametrization adopted in our model uses $sp^3d^5s^*$ orbitals in both the spin configurations and the values of the associated TB parameters for the Si and Ge crystal have been taken from Ref. 37 and 38, respectively. The SiGe barriers have been described by linear interpolation of the Si and Ge parameters. Finally, since the parametrization of Refs. 37, 38 holds at low temperature, a rigid shift of -90 meV of the conduction bands has been applied to take into account the temperature induced band-gap shrinkage. Following the procedure outlined in Ref. 39, the dipole matrix

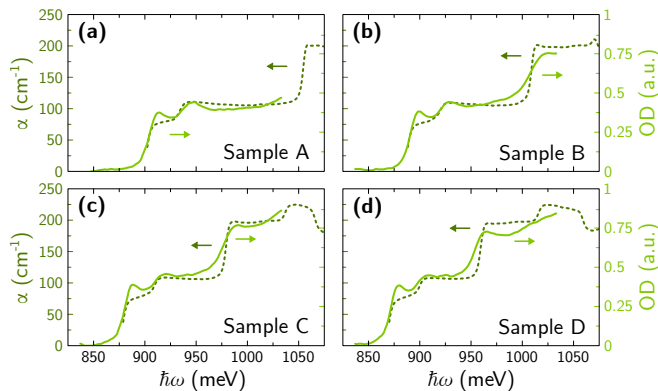


Figure 2. (color online) Calculated absorption coefficient (α , dark green dotted line) vs measured optical density (OD, light green continuous line) as a function of the photon energy for samples A to D [reported in panels (a-d), respectively].

elements have been expressed in terms of the hopping Hamiltonian parameters and of the first neighbor ion positions in the strained lattice. To calculate the spectrally resolved absorption coefficient and the optical polarization spectrum, the Ge/SiGe MQW Brillouin zone has been sampled in a neighbor of the Γ point with a grid featuring 800 nodes. Finally, to properly take into account the effects due to the coherent superposition of the double degenerate final states in the conduction band, the spin polarization along an arbitrary direction, induced by circularly polarized light propagating in the QW region with a given incidence angle, has been calculated as the expectation value of the density matrix operator, as reported for instance in Ref. 15.

In Fig. 1 (c) we show the experimental setup that we employ for the ISHE measurements. Optical orientation is performed exploiting the monochromatized light (typical bandwidth of 10 meV) of a super-continuum laser [40]. Within the reference frame of Fig. 1 (a), the Ohmic contacts can detect a current density \mathbf{j}_c parallel to the y -axis. The spin current density \mathbf{j}_s flows from the MQW to the Pt layer, thus it is directed along the z -axis [30–32]. Hence, eq. (1) imposes that ΔV_{ISHE} is sensitive only to the x -component of the spin polarization P_x (*i.e.*, P_{\parallel}). To get a significant P_x , the light beam illuminates the samples in an off-normal configuration. This is obtained by partially filling off-axis a 0.65 numerical aperture objective [10, 41, 42]. The light is focused on the sample with a polar angle $\vartheta \approx 30^\circ$, resulting in a polar angle inside the Ge layer $\vartheta_{\text{Ge}} \approx 6.6^\circ$, almost constant within the investigated photon energy range. The ISHE signal is measured with a lock-in amplifier by modulating the circular polarization of the light with a photo-elastic modulator (PEM) operating at 50 kHz [30, 31]. All the measurements have been performed at room temperature.

In Fig. 2 we report, for all the investigated samples, the comparison between the value of the absorption coefficient $\alpha(\hbar\omega)$ resulting from the calculation (dark green

dotted line) with the measured optical density (OD) of the MQWs (light green continuous line). The calculated absorption coefficient nicely matches the experimental measurement. The slight difference between the two is related to excitonic absorption peaks that we do not account in our calculations. Anyway, the comparison between predicted and measured absorption spectra let us to be confident with the reliability of our theoretical approach.

In Fig. 3 we report the value of ΔV_{ISHE} normalized to the flux of the incident photons Φ_{ph} . For all the samples we can identify two shoulders, highlighted in Fig. 3 with light blue arrows. From Tab. I we attribute the first shoulder to the overall contribution of $\text{HH1} \rightarrow \text{c}\Gamma 1$ and $\text{LH1} \rightarrow \text{c}\Gamma 1$ transitions and the second one to $\text{HH2} \rightarrow \text{c}\Gamma 2$. From sample A to sample D the energy difference between the two shoulders decreases, as expected, due to the increase of the well thickness.

The interpretation of the ISHE spectra is subject to the knowledge of the absorption coefficient and the initial spin-polarization of the quantum wells. Indeed, within a simple 1D spin drift-diffusion model, the dependence of ΔV_{ISHE} on α and P_x is expressed by the so-called Spicer-like formula [43] as:

$$\Delta V_{\text{ISHE}}(\hbar\omega) \propto P_x(\hbar\omega) \frac{\alpha(\hbar\omega) \ell_s}{1 + \alpha(\hbar\omega) \ell_s}, \quad (2)$$

with ℓ_s being the effective spin-diffusion length of the MQWs along an out-of-plane path. Here, in order to gain insight into the spectral dependence of the ISHE signals, we compute the value of P_x resulting from the same tight-binding model employed for the estimation of α (see Fig. 2). We report in Fig. 4 the component of the spin polarization at the time of generation projected

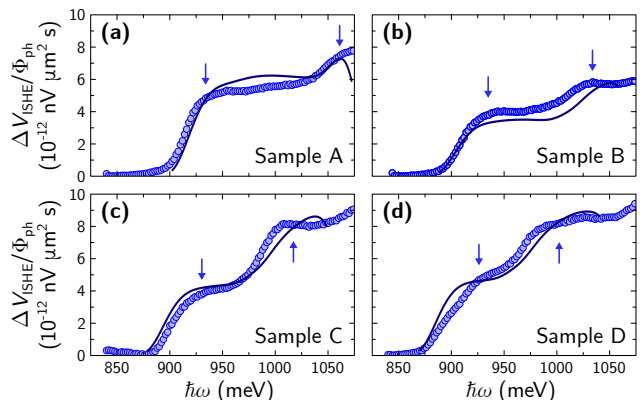


Figure 3. (color online) Experimental results (blue circles) of ΔV_{ISHE} normalized to the photon flux Φ_{ph} for the samples A to D [in panels (a-d), respectively]. The experimental error of the measurement is within the size of the circles. The dark blue line represents the fitting exploiting the model of Ref. 43, and is proportional to $P_x \alpha$ (calculated). The light blue arrows are placed close to the absorption edges of the MQWs.

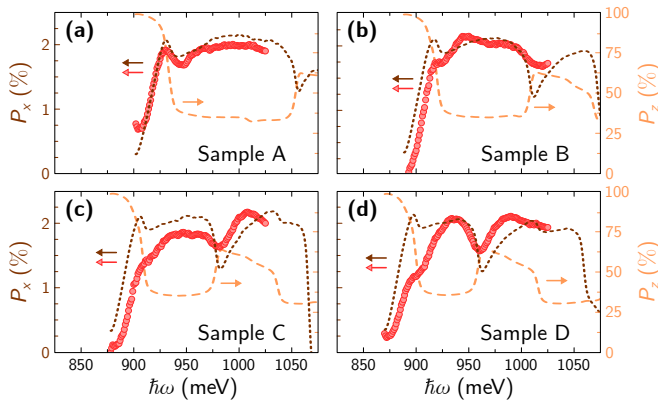


Figure 4. (color online) In-plane (P_x , brown dotted line) and out-of-plane (P_z , orange dashed line) component of the spin polarization as a function of the photon energy calculated for an incident angle $\vartheta_{\text{Ge}} = 6.6^\circ$ for samples A to D [respectively reported in panels (a-d)]. Red circles show the value of P_x extrapolated from experimental measurements as detailed in the text. Note the different spectral features of P_x and P_z , consequence of the symmetry reduction in MQWs.

along the x and z -axes [reference frame of Fig. 1 (b)], P_x (brown line) and P_z (orange line), respectively, calculated for $\vartheta_{\text{Ge}} = 6.6^\circ$. Since in MQWs the direction of the spin polarization \mathbf{u}_P is not parallel to the light wavevector \mathbf{k} due to the reduction of the symmetry, it is not possible to exploit the simple definition $P_x = P \sin \vartheta_{\text{Ge}}$ and the spectral shapes of P_x and P_z (*i.e.*, P_\perp) are different. The out-of-plane component reaches a value close to 100% for all the investigated samples, whether P_x remains almost constant around the value of 2% after the onset of the $\text{HH1} \rightarrow \text{c}\Gamma 1$ transitions, while a dip occurs in correspondence of the $\text{HH2} \rightarrow \text{c}\Gamma 2$ transition. Here, we point out that the small absolute value of P_x is related to the small polar angle ϑ_{Ge} exploited in our experimental geometry. The tight-binding model predicts values of P_x which could reach 20% as ϑ_{Ge} approaches 90° .

The dark blue line in Fig. 3 shows the best fit of $\Delta V_{\text{ISHE}}/\Phi_{\text{ph}}$ obtained with the Spicer-like model [eq. (2)]. We exploit the computed α and P_x parameters reported in Fig. 2 and 4, respectively, convoluted with a gaussian function accounting for both the thermal broadening of the energy states and the bandwidth of the light source. The best fit for all the investigated samples yields $\Delta V_{\text{ISHE}} \propto P_x \alpha$, which means that the Spicer-like model only provides the upper constrain $\ell_s \ll \alpha^{-1}$ [see eq. (2)]. In the investigated energy range, the maximum value of the absorption coefficient is $\alpha \approx 200 \text{ cm}^{-1}$, hence $\ell_s \ll \alpha^{-1} \approx 50 \text{ }\mu\text{m}$ for all the MQWs.

However, we can analyze the signal intensity to give a lower boundary estimation of ℓ_s . Indeed, *on one hand*, by dividing the measured $\Delta V_{\text{ISHE}}/\Phi_{\text{ph}}$ by the electric resis-

tance ($R_{\text{A-D}} \approx 200 \text{ }\Omega$) we get the value of the equivalent charge current $i_{\text{ISHE}}/\Phi_{\text{ph}}$ in the Pt layer. Then, if we assume $\gamma_{\text{Pt}} = 0.1$ [25–29] we can estimate the spin current i_s^{exp} needed to produce the detected ΔV_{ISHE} . *On the other hand*, we can also estimate the value of spin current i_s^{th} assuming that all the spins generated within a distance ℓ from the Pt/MQWs interface reach the interface. From Ref. 44 we have:

$$i_s^{\text{th}} = q \frac{W}{\hbar\omega} (1 - e^{-\alpha\ell}) P_x, \quad (3)$$

being W the light power transmitted to the MQW and q the elementary charge. Since the photon flux is $\Phi_{\text{ph}} = W/(\hbar\omega A)$, being A the area of the light beam, we get $i_s^{\text{th}}/\Phi_{\text{ph}} = q A (1 - e^{-\alpha\ell}) P_x$. Now, we can find the value of ℓ which allows the identity $i_s^{\text{exp}}/\Phi_{\text{ph}} = i_s^{\text{th}}/\Phi_{\text{ph}}$ to be respected. This value of ℓ would correspond to ℓ_s in absence of the built-in electric field at the metal/semiconductor junction. The presence of the Schottky barrier, instead, reduces the number of spin entering into Pt [45], hence $\ell_s > \ell$. We get $\ell \sim 200 \text{ nm}$ for all the investigated samples and photon energies, thus obtaining the lower boundary $\ell_s \gtrsim 200 \text{ nm}$ for vertical spin-transport in Ge/SiGe MQWs. It is worth mentioning that the range of ℓ_s we extract from our measurements is in agreement with previous estimations of the spin diffusion length in GaAs/AlGaAs quantum wells [46, 47].

For what concerns the spin-polarization, exploiting the Spicer-like model we concluded that $\Delta V_{\text{ISHE}} = c P_x \alpha$, with c a proper proportionality constant known from the best fit. This means that with the measurements of ΔV_{ISHE} and of the OD (properly scaled to fit the calculated α values) and using the c value estimated from the Spicer-like model, we can directly estimate P_x . In Fig. 4 we report the results of the procedure. Notably, this experimentally-inferred P_x nicely agrees with the calculated one, for all the investigated samples. In particular, the comparison between the two is good for samples A and B, while, from the theoretical predictions, a slightly larger value of P_x should be expected below 925 meV for samples C and D. In any case, we conclude that the measurement of ΔV_{ISHE} can be exploited to directly access information about the in-plane spin polarization which, to the best of our knowledge, is inaccessible to other experimental techniques.

In conclusion, we exploit a spin injection/detection scheme in a Pt/MQWs system, based on optical orientation of spin-polarized electrons in the quantum wells, and ISHE detection in the Pt layer. This allows us to expect for all the investigated MQWs a spin-diffusion length ℓ_s in the range between hundreds of nanometers and few micrometers for vertical spin transport. More importantly, the sensitivity of the technique let us directly estimating from experimental measurements the value of the in-plane spin-polarization, which nicely agrees with theoretical predictions.

- [1] J. Fabian, A. Matos-Abiague, C. Ertler, P. Stano, and I. Žutić, Semiconductor spintronics, *Acta Physica Slovaca. Reviews and Tutorials* **57**, 10.2478/v10155-010-0086-8 (2007).
- [2] D. D. Awschalom and M. E. Flattè, Challenges for semiconductor spintronics, *Nature Physics* **3**, 153 (2007).
- [3] M. Dyakonov, *Spin Physics in Semiconductors* (Springer, 2008) pp. 211–244.
- [4] C. Zucchetti, F. Bottegoni, C. Vergnaud, F. Ciccacci, G. Isella, L. Ghirardini, M. Celebrano, F. Rortais, A. Ferrari, A. Marty, M. Finazzi, and M. Jamet, Imaging spin diffusion in germanium at room temperature, *Physical Review B* **96**, 014403 (2017).
- [5] F. Bottegoni, C. Zucchetti, S. Dal Conte, J. Frigerio, E. Carpena, C. Vergnaud, M. Jamet, G. Isella, F. Ciccacci, G. Cerullo, and M. Finazzi, Spin-hall voltage over a large length scale in bulk germanium, *Physical Review Letters* **118**, 167402 (2017).
- [6] K. Hamaya, Y. Fujita, M. Yamada, M. Kawano, S. Yamada, and K. Sawano, Spin transport and relaxation in germanium, *Journal of Physics D: Applied Physics* **51**, 393001 (2018).
- [7] C. Zucchetti, M. Bollani, G. Isella, M. Zani, M. Finazzi, and F. Bottegoni, Doping dependence of the electron spin diffusion length in germanium, *APL Materials* **7**, 101122 (2019).
- [8] J. Rioux and J. E. Sipe, Optical injection and control in germanium: Thirty-band $\mathbf{k} \cdot \mathbf{p}$ theory, *Physical Review B* **81**, 155215 (2010).
- [9] J.-C. Rojas-Sánchez, M. Cubukcu, A. Jain, C. Vergnaud, C. Portemont, C. Ducruet, A. Barski, A. Marty, L. Vila, J.-P. Attané, E. Augendre, G. Desfonds, S. Gambarelli, H. Jaffrès, J.-M. George, and M. Jamet, Spin pumping and inverse spin hall effect in germanium, *Physical Review B* **88**, 064403 (2013).
- [10] C. Zucchetti, F. Bottegoni, G. Isella, M. Finazzi, F. Rortais, C. Vergnaud, J. Widiez, M. Jamet, and F. Ciccacci, Spin-to-charge conversion for hot photoexcited electrons in germanium, *Physical Review B* **97**, 125203 (2018).
- [11] C. Zucchetti, M.-T. Dau, F. Bottegoni, C. Vergnaud, T. Guillet, A. Marty, C. Beigné, S. Gambarelli, A. Picone, A. Calloni, G. Bussetti, A. Brambilla, L. Duò, F. Ciccacci, P. K. Das, J. Fujii, I. Vobornik, M. Finazzi, and M. Jamet, Tuning spin-charge interconversion with quantum confinement in ultrathin bismuth films, *Physical Review B* **98**, 184418 (2018).
- [12] Y. A. Bychkov and E. I. Rashba, Properties of a 2D electron gas with lifted spectral degeneracy, *JETP Letters* **39** (1984).
- [13] V. Edelstein, Spin polarization of conduction electrons induced by electric current in two-dimensional asymmetric electron systems, *Solid State Communications* **73**, 233 (1990).
- [14] D. T. Pierce and F. Meier, Photoemission of spin-polarized electrons from GaAs, *Physical Review B* **13**, 5484 (1976).
- [15] F. Meier and B. P. Zakharchenya, *Optical Orientation* (Elsevier, 1984).
- [16] F. Bottegoni, A. Ferrari, G. Isella, S. Cecchi, M. Marcon, D. Chrastina, G. Trezzi, and F. Ciccacci, Ge/sige heterostructures as emitters of polarized electrons, *Journal of Applied Physics* **111**, 063916 (2012), <https://doi.org/10.1063/1.3698290>.
- [17] F. Pezzoli, F. Bottegoni, D. Trivedi, F. Ciccacci, A. Giorgioni, P. Li, S. Cecchi, E. Grilli, Y. Song, M. Guzzi, H. Dery, and G. Isella, Optical spin injection and spin lifetime in ge heterostructures, *Phys. Rev. Lett.* **108**, 156603 (2012).
- [18] G. Bastard, *Wave mechanics applied to semiconductor heterostructures* (John Wiley and Sons Inc, 1990).
- [19] T. Jungwirth, J. Wunderlich, and K. Olejník, Spin Hall effect devices, *Nature Materials* **11**, 382 (2012).
- [20] P. Chaisakul, D. Marris-Morini, J. Frigerio, D. Chrastina, M.-S. Rouifed, S. Cecchi, P. Crozat, G. Isella, and L. Vivien, Integrated germanium optical interconnects on silicon substrates, *Nature Photonics* **8**, 482 (2014).
- [21] M. Rouifed, D. Marris-Morini, P. Chaisakul, J. Frigerio, G. Isella, D. Chrastina, S. Edmond, X. Le Roux, J. Coudeville, D. Bouville, and L. Vivien, Advances toward ge/sige quantum-well waveguide modulators at 1.3 μm , *IEEE Journal of Selected Topics in Quantum Electronics* **20**, 33 (2014).
- [22] G. Lampel, Nuclear dynamic polarization by optical electronic saturation and optical pumping in semiconductors, *Physical Review Letters* **20**, 491 (1968).
- [23] M. Dyakonov and V. Perel, Possibility of orienting electrons spins with current, *JETP Letters* **13**, 467 (1971).
- [24] M. Dyakonov and V. Perel, Current-induced spin orientation of electrons in semiconductors, *Physics Letters A* **35**, 459 (1971).
- [25] K. Ando, S. Takahashi, K. Harii, K. Sasage, J. Ieda, S. Maekawa, and E. Saitoh, Electric manipulation of spin relaxation using the spin hall effect, *Phys. Rev. Lett.* **101**, 036601 (2008).
- [26] A. Azevedo, L. H. Vilela-Leão, R. L. Rodríguez-Suárez, A. F. Lacerda Santos, and S. M. Rezende, Spin pumping and anisotropic magnetoresistance voltages in magnetic bilayers: Theory and experiment, *Phys. Rev. B* **83**, 144402 (2011).
- [27] W. Zhang, V. Vlaminck, J. E. Pearson, R. Divan, S. D. Bader, and A. Hoffmann, Determination of the pt spin diffusion length by spin-pumping and spin hall effect, *Applied Physics Letters* **103**, 242414 (2013), <https://doi.org/10.1063/1.4848102>.
- [28] M. Obstbaum, M. Härtinger, H. G. Bauer, T. Meier, F. Swientek, C. H. Back, and G. Woltersdorf, Inverse spin hall effect in $\text{ni}_{81}\text{fe}_{19}$ /normal-metal bilayers, *Phys. Rev. B* **89**, 060407 (2014).
- [29] M. Isasa, E. Villamor, L. E. Hueso, M. Gradhand, and F. Casanova, Temperature dependence of spin diffusion length and spin hall angle in au and pt, *Phys. Rev. B* **91**, 024402 (2015).
- [30] K. Ando, M. Morikawa, T. Trypiniotis, Y. Fujikawa, C. H. W. Barnes, and E. Saitoh, Direct conversion of light-polarization information into electric voltage using photoinduced inverse spin-Hall effect in Pt/GaAs hybrid structure: Spin photodetector, *Journal of Applied Physics* **107**, 113902 (2010).
- [31] F. Bottegoni, A. Ferrari, G. Isella, M. Finazzi, and F. Ciccacci, Experimental evaluation of the spin-Hall conductivity in Si-doped GaAs, *Physical Review B* **88**, 121201 (2013).

- [32] F. Bottegoni, C. Zucchetti, F. Ciccacci, M. Finazzi, and G. Isella, Optical generation of pure spin currents at the indirect gap of bulk si, *Applied Physics Letters* **110**, 042403 (2017).
- [33] G. Isella, D. Chrastina, B. Rössner, T. Hackbarth, H.-J. Herzog, U. König, and H. von Känel, Low-energy plasma-enhanced chemical vapor deposition for strained si and ge heterostructures and devices, *Solid-State Electronics* **48**, 1317 (2004), strained-Si Heterostructures and Devices.
- [34] D. Aspnes, Third-derivative modulation spectroscopy with low-field electroreflectance, *Surface Science* **37**, 418 (1973).
- [35] M. Virgilio, M. Bonfanti, D. Chrastina, A. Neels, G. Isella, E. Grilli, M. Guzzi, G. Grosso, H. Sigg, and H. von Känel, Polarization-dependent absorption in ge/sige multiple quantum wells: Theory and experiment, *Phys. Rev. B* **79**, 075323 (2009).
- [36] M. Virgilio and G. Grosso, Quantum-confined stark effect in ge/sige quantum wells: A tight-binding description, *Phys. Rev. B* **77**, 165315 (2008).
- [37] J.-M. Jancu, R. Scholz, F. Beltram, and F. Bassani, Empirical *spds** tight-binding calculation for cubic semiconductors: General method and material parameters, *Phys. Rev. B* **57**, 6493 (1998).
- [38] J.-M. Jancu and P. Voisin, Tetragonal and trigonal deformations in zinc-blende semiconductors: A tight-binding point of view, *Phys. Rev. B* **76**, 115202 (2007).
- [39] F. Trani, G. Cantele, D. Ninno, and G. Iadonisi, Tight-binding calculation of the optical absorption cross section of spherical and ellipsoidal silicon nanocrystals, *Phys. Rev. B* **72**, 075423 (2005).
- [40] SuperK Extreme EXW-12, NKT Photonics. The laser delivers nanoseconds pulses at a 78 MHz repetition rate in the $0.7 \div 2.2$ eV range. Here, we do not exploit the temporal structure of the laser source. Indeed, our results are time-averaged since the temporal average of the time-dependent spin drift-diffusion equation equals the solution for the spin drift-diffusion equation in the steady-state, see Ref. 45.
- [41] M. Savoini, F. Ciccacci, L. Duò, and M. Finazzi, Apparatus for vectorial Kerr confocal microscopy, *Review of Scientific Instruments* **82**, 023709 (2011).
- [42] C. Stamm, C. Murer, M. Berritta, J. Feng, M. Gabureac, P. M. Oppeneer, and P. Gambardella, Magneto-optical detection of the spin hall effect in pt and w thin films, *Physical Review Letters* **119**, 087203 (2017).
- [43] F. Bottegoni, C. Zucchetti, G. Isella, E. Pinotti, M. Finazzi, and F. Ciccacci, Modeling the photo-induced inverse spin-hall effect in pt/semiconductor junctions, *Journal of Applied Physics* **124**, 033902 (2018).
- [44] G. Isella, F. Bottegoni, A. Ferrari, M. Finazzi, and F. Ciccacci, Photon energy dependence of photo-induced inverse spin-hall effect in pt/gaas and pt/ge, *Applied Physics Letters* **106**, 232402 (2015).
- [45] C. Zucchetti, G. Isella, F. Ciccacci, M. Finazzi, and F. Bottegoni, Spin transport and spin-charge interconversion phenomena in Ge-based structures, in *Spintronics XII*, Vol. 11090, edited by H.-J. M. Drouhin, J.-E. Wegrowe, and M. Razeghi, International Society for Optics and Photonics (SPIE, 2019) pp. 73 – 82.
- [46] C. Hu, H. Ye, G. Wang, H. Tian, W. Wang, W. Wang, B. Liu, and X. Marie, Room temperature spin diffusion in (110) GaAs/AlGaAs quantum wells, *Nanoscale Research Letters* **6**, 149 (2011).
- [47] G. Wang, B. L. Liu, A. Balocchi, P. Renucci, C. R. Zhu, T. Amand, C. Fontaine, and X. Marie, Gate control of the electron spin-diffusion length in semiconductor quantum wells, *Nature Communications* **4**, 2372 (2013).